JMEPEG (2007) 16:123–130
DOI: 10.1007/s11665-006-9020-0

1059-9495/$19.00

The Influence of Centerline Sigma (σ) Phase on the Through-Thickness Toughness and Tensile Properties of Alloy AL-6XN

K.D. Adams, J.N. DuPont, and A.R. Marder

(Submitted June 12, 2006)

The *J*-integral fracture toughness and tensile behavior of AL-6XN (ATI Properties Inc., Pittsburgh, PA, USA) plate material in the short-transverse (S-T) orientation was studied. The material was tested with respect to the presence or absence of microstructural 'packets' of brittle sigma phase (σ-phase) particles within the austenite matrix, located near the centerline of the plate. The *J*-integral-fracture resistance curve (*J-R*-curve) qualitatively indicated that the presence of the σ-phase packets is a detriment to the fracture toughness of the material in the S-T orientation. Tensile specimens containing the packets of σ-phase particles exhibited reduced yield and tensile strengths as well as pronounced reduction in ductility compared to specimens nominally free of σ-phase packets. Particle cracking was observed within the σ-phase packets, which lead to premature fracture. This limited the ability of the material to plastically deform and work-harden, thereby accounting for the observed reductions in ductility, toughness, and ultimate tensile strength.

Keywords AL-6XN, Fracture toughness, *J*-integral, *J-R* curve, Sigma phase, Tensile

1. Introduction

Super austenitic stainless steel alloys, such as AL-6XN, are used in a variety of applications that require a combination of good toughness and corrosion resistance. The corrosion resistance of these alloys is improved over conventional stainless steels, in part, by the additions of Mo at about 6-7 wt.% (Ref 1). While the addition of this element improves corrosion resistance, it also can lead to the formation of σ-phase in the centerline of plates that are continuously cast. The σ-phase is a Cr/Mo rich intermetallic that is brittle and has been shown to be detrimental to the tensile properties of alloy AL-6XN (Ref 2). Although a detailed study has not been published on the exact formation mechanism of the centerline σ-phase, it is well known (Ref 3) that Mo segregates strongly to the liquid during solidification of alloy AL-6XN and that solidification terminates by a eutectic type $L \rightarrow \gamma/\sigma$ reaction. Since the σ-phase forms in the centerline of the plate where the Mo concentration is expected to be the highest due to segregation, its formation is likely associated with the final solidification product.

The influence of brittle second phase particles on the mechanical properties of engineering alloys has been studied in many other systems. For example, Wang recently (Ref 4) considered the fracture process concerning brittle Fe-rich intermetallic and Si-based particles in a ductile aluminum matrix and found that the particle size, shape, and distribution greatly affect the mechanism of fracture in such materials. The general sequence of events observed were: (1) shear band formation in the ductile matrix at the initial stage of straining, (2) particle cracking due to dislocation pileup at particles from continued straining, (3) micro-crack formation between cracked particles upon further straining, and (4) rapid linkage of micro-cracks when a critical volume fraction of cracked particles is reached. Thus, particle cracking is known to accelerate the fracture process, leading to reduced ductility and toughness. It has generally been shown (Ref 5) that: (1) larger particles are more likely to crack because the fracture stress for larger particles is smaller due to a higher probability of the presence of larger defects, (2) particles with larger aspect ratios are more likely to crack since the particle stress is proportional to the aspect ratio and dislocations have difficulty cross-slipping around them, and (3) the occurrence of multiple-cracking of particles is an indication that the particle/matrix interface is strong since the cracks are formed by stresses applied to the particle by the matrix.

Although it has been shown that σ-phase can be detrimental in the short-transverse compared to the longitudinal or long-transverse loading conditions in alloy AL-6XN (Ref 2), the influence of centerline σ-phase on the through-thickness toughness and tensile properties has not been isolated from effects of anisotropy due to rolling. Thus, the purpose of this study is to determine the effects of centerline σ-phase packets on the through-thickness mechanical properties of this alloy.

2. Experimental Procedure

The AL-6XN used in this study includes 25.4-mm-thick plate material for mechanical testing in the through-thickness

K.D. Adams, J.N. DuPont, and **A.R. Marder,** Materials Science and Engineering, Lehigh University, 5 East Packer Ave, Bethlehem, PA 18015, USA. Contact e-mail: kda3@lehigh.edu.

(short-transverse) orientation and 15.9-mm-thick plate for testing in the longitudinal and transverse orientations for comparison. The composition of each plate of AL-6XN is given in Table 1. Both materials were observed to contain microstructural "packets" of σ-phase particles near the centerline of the plates. A typical example of this for each plate is shown in Fig. 1; Fig. 1(a) and (b) correspond to longitudinal and transverse cross-sections of the 25.4-mm-thick plate, respectively, and Fig. 1(c) and (d) correspond to longitudinal and transverse cross-sections of the 15.9-mm-thick plate, respectively. To obtain AL-6XN "σ-free" samples, material was saw-cut approximately 7.6-mm from the surface of the 25.4-mm-thick plate material, since σ-phase packets were nominally absent in this region, see Fig. 1(e). (In this work, "σ-free" refers to material that does not contain packets of conglomerated σ-phase particles at the centerline. However, σ-free samples can still contain small amounts of isolated σ particles.) In order to test the through-thickness mechanical properties of both σ-containing and σ-free material, extensions of AL-6XN were electron-beam (e-beam) welded to the top and bottom surfaces of these sections as shown schematically in Fig. 2. The electron-beam welding was conducted using a beam power of ~2200 W and a travel speed of 4–6 mm/s.

Table 1 Elemental composition of both AL-6XN plate materials used

Element, wt.%	25.4-mm-thick plate	15.9-mm-thick plate
C	0.02	0.02
Mn	0.51	0.38
P	0.016	0.016
S	0.001	0.001
Si	0.46	0.50
Cr	20.54	20.69
Ni	24.31	24.06
Mo	6.01	6.11
N	0.22	0.22
Cu	0.19	0.20
Co	0.12	0.11
Fe	Balance	Balance

Standard compact tension $C(T)$ specimens were prepared from the e-beam welded samples for J-integral fracture toughness testing having 12.7-mm-thickness and 50.8-mm-width (measured from the load-line to the end of the specimen). For specimens used to test through-thickness properties, the starter notch was oriented parallel to the centerline of the plate material and the load was applied perpendicular to that. Specimens used to test properties in the longitudinal and transverse directions with respect to the rolling direction (from the 15.9-mm-thick plate) were oriented with the notch parallel and perpendicular to the rolling direction, respectively, and the load was applied within the plane of the plate, perpendicular to the notch.

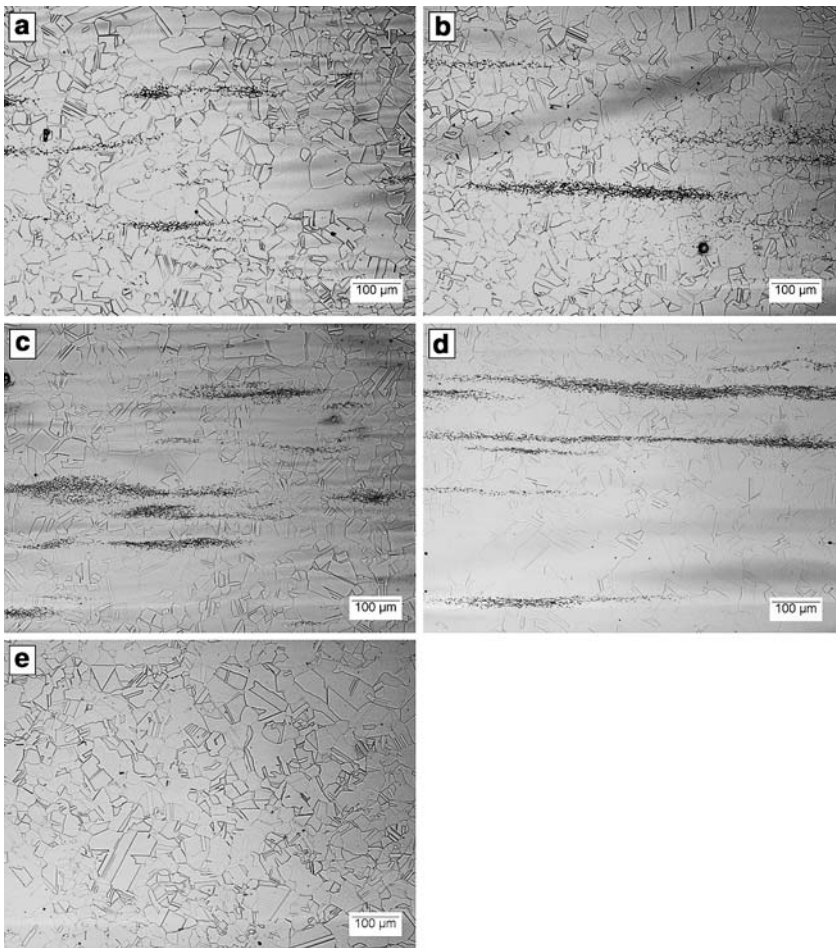

Fig. 1 Typical microstructures of the 25.4-mm-thick plate material (a) in longitudinal cross-section, (b) in transverse cross-section; the 12.7-mm-thick plate material (c) in longitudinal cross-section, (d) in transverse cross-section; and (e) the region of the 25.4-mm-thick plate that corresponds to the σ-free samples (light optical microscope images)

"Dog-bone" type tensile specimens were fabricated in a manner similar to the *C*(*T*) specimens. As shown schematically in Fig. 3, the tensile samples were prepared with a double-reduced gauge length. This sample configuration was based on preliminary tests and was designed to concentrate the plastic deformation within the zone containing the material oriented in the short-transverse direction. The sample dimensions were chosen so that the second reduced cross-section would reach the ultimate tensile strength of the material before the first reduced cross-section reached the yield stress. The gauge-length was consistent for both σ-containing and σ-free samples. Longitudinal and transverse orientations were not tested since a similar study had been done previously (Ref 2).

The sample orientation designations and corresponding interaction of the crack plane with the σ-phase packets are consistent with ASTM E399 classifications (Ref 6). The S-T(σ-containing) orientation designates the short-transverse orientation containing the packets of σ-phase particles. S-T(σ-free) designates the short-transverse orientation that is nominally free of the packets of σ-phase particles. T-L and L-T designate the longitudinal and transverse orientations relative to the rolling direction of the plate, respectively, as described in Ref 6.

Tensile tests were performed in accordance with Ref 7, except for the double-reduced cross-section configuration. A 12.7-mm extensometer was used for strain measurements and the final elongation measurements were made using original gauge marks 6.35-mm apart. The yield strength was determined using the 0.2%-offset method with a cross-head speed of 0.508-mm/s. A 5.08-mm/s cross-head speed was used to reach final fracture.

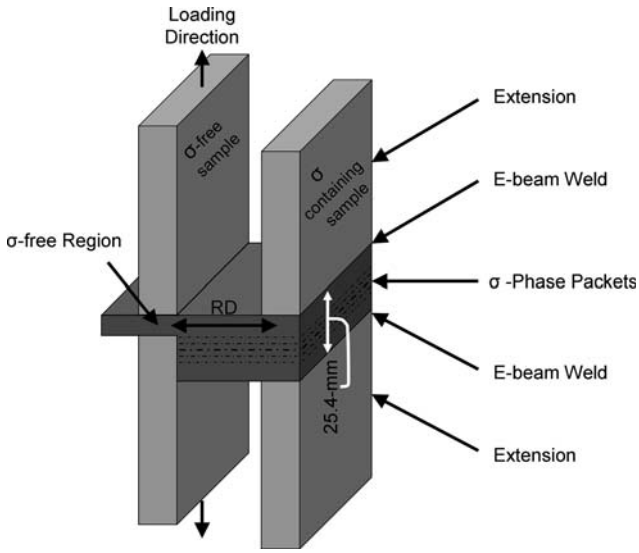

Fig. 2 Schematic representation of how the samples were obtained in the through-thickness (short-transverse) direction. The rolling direction (RD) of the through-thickness section is indicated

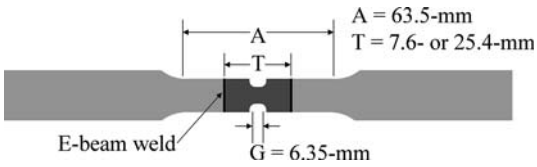

Fig. 3 Tensile sample dimensions, showing the gauge length (*G*) of the second reduced-cross-section within the through-thickness plate material (*T*) in comparison to the first reduced-cross-section (*A*). *T* = 7.6-mm for the σ-free samples and *T* = 25.4-mm for the σ-containing samples. Electron beam welds join the central (short-transverse oriented) piece to the outer (extension) pieces of the same material

J-integral fracture toughness testing using the resistance curve approach was conducted in accordance with (Ref 8) in duplicate for each of the four *C*(*T*) specimen conditions: S-T(σ-containing), S-T(σ-free), T-L, and L-T. The *J*-integral was used instead of the stress-intensity factor, *K*, as a fracture criterion since the sample size requirements for valid K_{IC} fracture toughness testing as noted in (Ref 6) were not met. For a valid plane-strain facture toughness test, according to the ASTM standard, the σ_Y/E ratio for AL-6XN would require a nominal specimen thickness much greater than 7.62-cm, which was not feasible due to fabrication limitations. (σ_Y and *E* are the yield stress and modulus of elasticity, respectively). Additionally, side-grooves were employed since they tend to make the *J*-integral more uniform at the crack-tip across the thickness of the specimen (Ref 9). The tests were performed using an MTS-brand (MTS Systems Corporation, Eden Prairie, MN, USA) 100 kN servo-hydraulic uniaxial loading system and a MTS 458 controller. A computer integrated to the controller was used to analyze the raw data for fracture toughness calculations and to report various information to a PC running software developed by Fracture Technology Associates, Inc. (FTA, Bethlehem, PA, USA.). The computer monitored the load applied to the specimen, which was accomplished by the use of standard 1.0T compact tension clevises with flat-bottomed holes attached to the cross-head and hydraulic ram of the test system, and the load-line displacement, as measured by a MTS 632.03B-30 clip gauge. *J* was calculated using the load–load-line-displacement records, as treated in (Ref 8), and the corresponding crack lengths were calculated using in situ compliance measurements. *R*-curves (*J*-Δ*a*) were generated for each specimen geometry.

Samples for metallographic examination were prepared using standard techniques and electrolytically etched using a solution of 60% HNO_3 and 40% H_2O with a potential of 1-3 V for approximately 5-10 s using a Pt electrode. Light optical microscopy (LOM) and scanning electron microscopy (SEM) techniques were used for microstructural characterization. SEM was conducted on a Philips (Koninklijke Philips Electronics N.V., The Netherlands) XL30 scanning electron microscope with an accelerating voltage of 10-20 kV.

3. Results and Discussion

Figure 4 shows the *J*-*R* curve representation of the *J*-integral fracture toughness data for the S-T(σ-containing), S-T(σ-free), L-T, and T-L sample orientations. It is important to recognize that these results are qualitative in nature since the sample sizes limited the region of valid data (dashed rectangle), in accordance with Ref 8, to values below which the differences in the fracture response of the samples are apparent. According to the standard (Ref 8), the maximum *J*-integral capacity for a specimen is given by the smaller of the following: $J_{max} = b\sigma_Y/20$ or $J_{max} = B\sigma_Y/20$, where $\sigma_Y = (\sigma_{YS} + \sigma_{TS})/2$, σ_{YS} = yield stress, σ_{TS} = ultimate tensile stress, *b* is the remaining uncracked ligament of the sample (width *W* − crack length *a*),

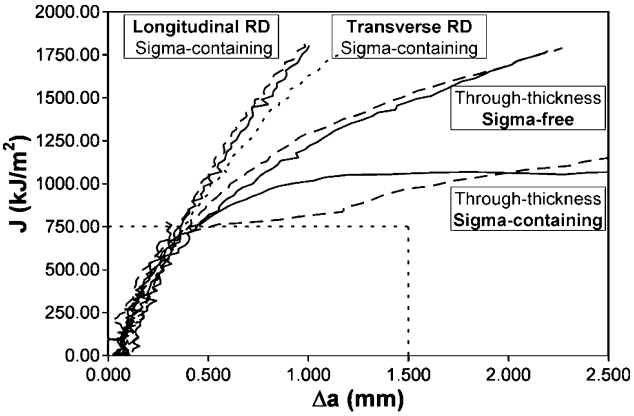

Fig. 4 *J-R* curve fracture toughness data for the S-T(σ-containing and σ-free), L-T, and T-L sample orientations

and B is the specimen thickness. This "limit" to the valid data is somewhat conservative considering that the requirements for plane-strain conditions for J testing occurs when $J \leq B\sigma_{YS}$ (Ref 10). Additionally, the maximum crack extension capacity for a specimen is given by the following: $\Delta a_{max} = 0.25b_0$, where b_0 is the original remaining ligament (width W − original crack length). In order to determine valid J_{IC} values, the 0.2-mm off-set construction line (parallel to and off-set from the blunting line) must intersect the J-Δa curve within the region of valid data described above. This indicates that for the data shown in Fig. 4, valid J_{IC} values could have been determined had the samples been large enough to move the dashed lines to values larger than the data experienced during the test. Although these results cannot be viewed in a quantitative manner according to these restrictions, they still indicate there is a significant difference in the toughness of AL-6XN as affected by the sample orientation and presence of σ-phase.

LOM photomicrographs that compare the cross-sectional views of cracking in the through-thickness J-integral fracture toughness samples are shown in Fig. 5. It is clear that the crack preferentially grows along σ-phase packets (Fig. 5a), whereas significant crack blunting occurs when these packets are not present (Fig. 5b). The crack appears to travel from one packet to another, either because (1) the previous packet it was traveling along ended or (2) a micro-crack had likely already formed within a packet on a different plane which linked to the macro-crack. A SEM photomicrograph of an area adjacent to the crack is shown in Fig. 6, and the extensive particle cracking near the fracture surface is readily apparent. The high level of Cr and Mo shown by the energy dispersive spectrum (EDS) collected from a σ-particle (Fig. 6b) compared to the matrix (Fig. 6c) supports the view that the particles are σ-phase, consistent with previous results (Ref 11). The fracture surfaces of the σ-containing and σ-free through-thickness samples are shown in Fig. 7 and 8. Here, the fracture surface of the σ-containing sample exhibits discrete plateaus that form when the crack moves from one packet of σ-phase particles to another. This is consistent with the cross-sectional fracture morphology shown in Fig. 5.

The toughness in the longitudinal and transverse rolling directions is greater than both through-thickness conditions even though σ-phase is present in these samples. This is obviously attributed to sample orientation effects. The portion of the crack front that encounters the σ-phase packets in the longitudinal and transverse orientations is very small compared to the through-thickness σ-containing samples. This is further exemplified by observing that the through-thickness σ-free samples exhibited qualitatively lower toughness values compared to the longitudinal and transverse samples. From this it is apparent that (1) anisotropy from rolling and (2) the presence of σ-phase packets both affect the toughness of AL-6XN.

Table 2 shows the tensile data for the S-T(σ-containing) and S-T(σ-free) sample orientations. The σ-free samples show higher and more consistent strength and ductility compared to the σ-containing samples. Cross-sectional LOM and SEM photomicrographs of the tensile fractures are shown in Fig. 9 (σ-containing) and 10 (σ-free). The σ-containing sample exhibited a flat fracture with little evidence of plastic deformation, and the fracture appears to follow the σ-phase packets. Higher magnification examination (Fig. 9b) shows evidence of particle cracking just below the fracture surface, correlated to the cracked particles in Fig. 6. By comparison, the σ-free sample exhibits gross plastic deformation as evident by the appearance of grains elongated in the loading direction (Fig. 10a). Microvoids from the σ-free sample exhibited individual σ-particles that initiated the voids (Fig. 10b). These microvoids occurred as a result of the dispersed individual σ-particles.

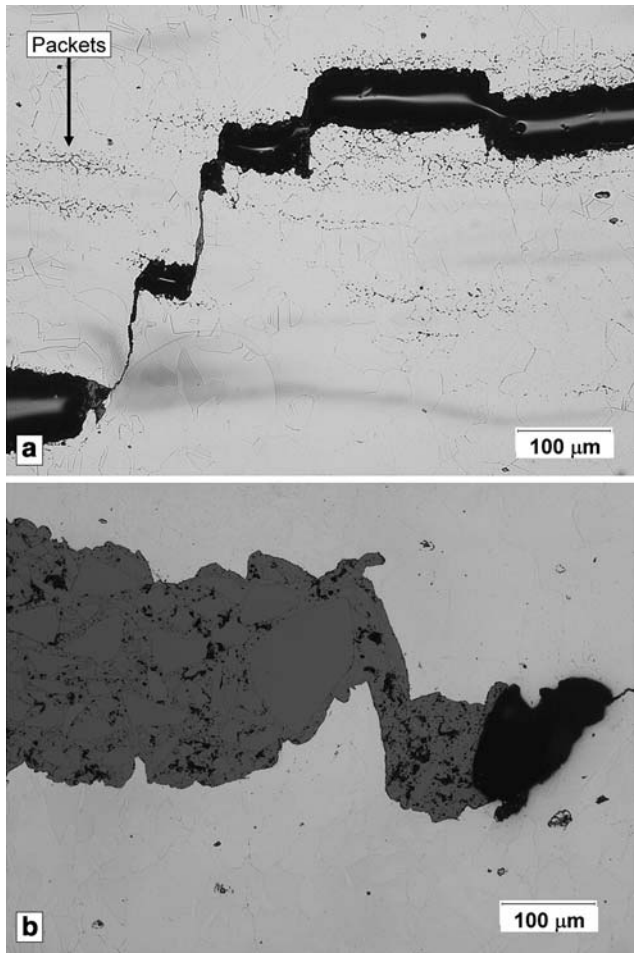

Fig. 5 Microstructural cross-sections of the (a) σ-containing and (b) σ-free fracture toughness samples post-test (light optical microscope images)

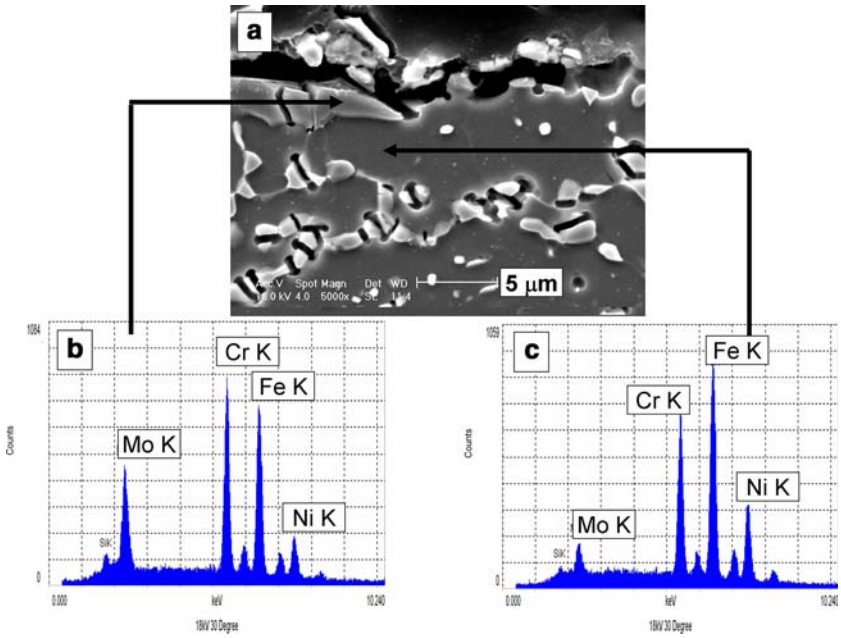

Fig. 6 (a) Scanning electron microscope image of the cross-section of a -ã-containing fracture toughness sample showing cracked particles; EDS data for (b) a particle, and (c) the austenite matrix

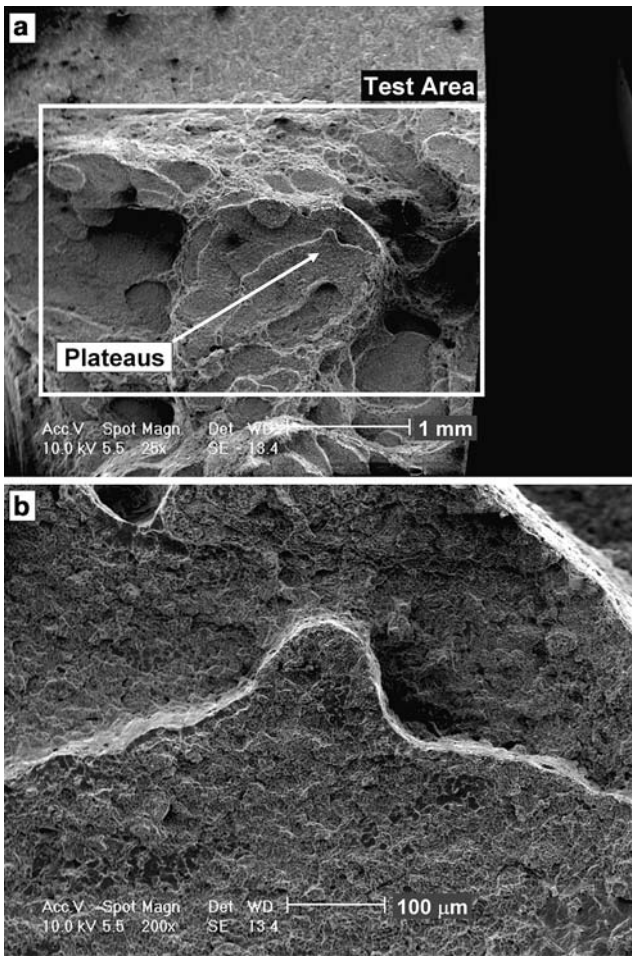

Fig. 7 The fracture surface appearance of a σ-containing S-T fracture toughness sample as viewed in the scanning electron microscope: (a) 25× and (b) 200× magnification. The white rectangle indicates the fracture surface created during the test

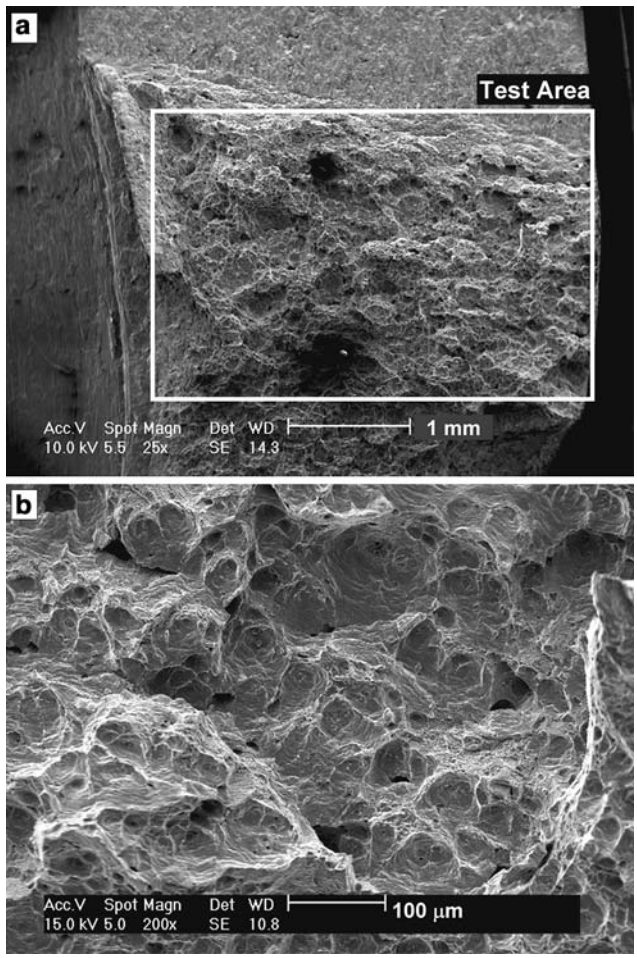

Fig. 8 The fracture surface appearance of a σ-free S-T fracture toughness sample as viewed in the scanning electron microscope: (a) 25× and (b) 200× magnification. Microvoid coalescence is apparent in (b). The white rectangle indicates the fracture surface created during the test

Table 2 Tensile data for the two through-thickness conditions: σ-containing and σ-free

Sample	Tensile strength, MPa	Yield strength, MPa	Elongation, %	Reduction in area, %
Sigma-containing	793	421	38	28
Sigma-containing	569	455	12	10
Sigma-free	862	497	76	65
Sigma-free	855	486	79	65

Typical fracture surfaces of the tensile samples are shown in Fig. 11 and 12. The fracture surface of the σ-containing sample (Fig. 11a) exhibits plateaus, which are indicative of the crack moving from the plane of one σ-phase packet to another. Closer inspection of the surface of the plateaus reveals cracked σ-phase particles (Fig. 11b and c) correlating to the cracked particles seen in cross-section (Fig. 9b). By comparison, the fracture surface of the σ-free sample (Fig. 12) displays typical microvoid coalescence, which corroborates with the large amount of plastic deformation observed for this sample orientation. The size of the microvoids in the σ-free sample appear to be bimodal. This can probably be attributed to the presence of well-dispersed isolated σ-phase particles that nucleate fewer, more widely spaced voids.

From these observations, the detrimental effect of centerline σ-phase packets on the through-thickness toughness and tensile properties of AL-6XN is readily apparent. When the packets of σ-phase are present only as isolated particles in small amounts, the austenite matrix grains are able to plastically deform extensively and failure occurs by a typical microvoid coalescence mechanism. However, when the σ-phase is present as packets with a high population of σ particles that undergo particle cracking, the ability of the material to plastically deform is significantly reduced. This accounts for the relatively low ductility and toughness as well as the low tensile strength data. The low tensile strengths can be attributed to the inability of the σ-containing samples to work harden due to early fracture associated with the σ particles.

As mentioned previously, Stauffer et al. (Ref 2) studied the tensile properties of AL-6XN that contained σ-phase packets similar to that observed here. Testing was conducted in various orientations and it was found that the ductility in the short-transverse orientation was much lower than that for the longitudinal or long-transverse loading directions. The decrease in ductility associated with the presence of the σ-phase was

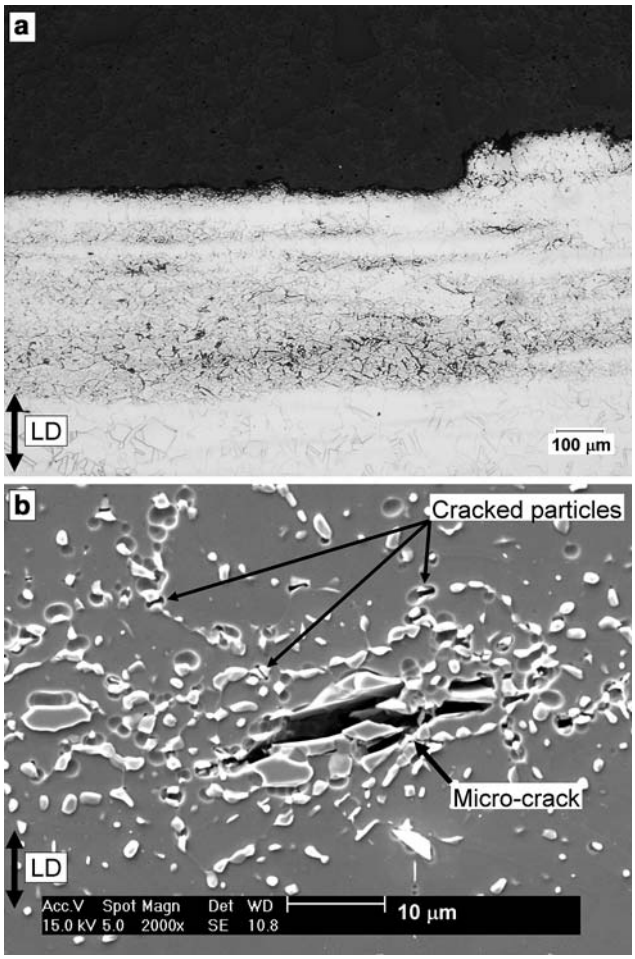

Fig. 9 Cross-sections near the fracture surface of (a) a σ-containing tensile sample (light optical microscope image) and (b) a σ-containing sample exhibiting a micro-crack that formed due to the fracture of a large particle, also showing cracked individual particles (scanning electron microscope image). Loading direction (LD) is indicated

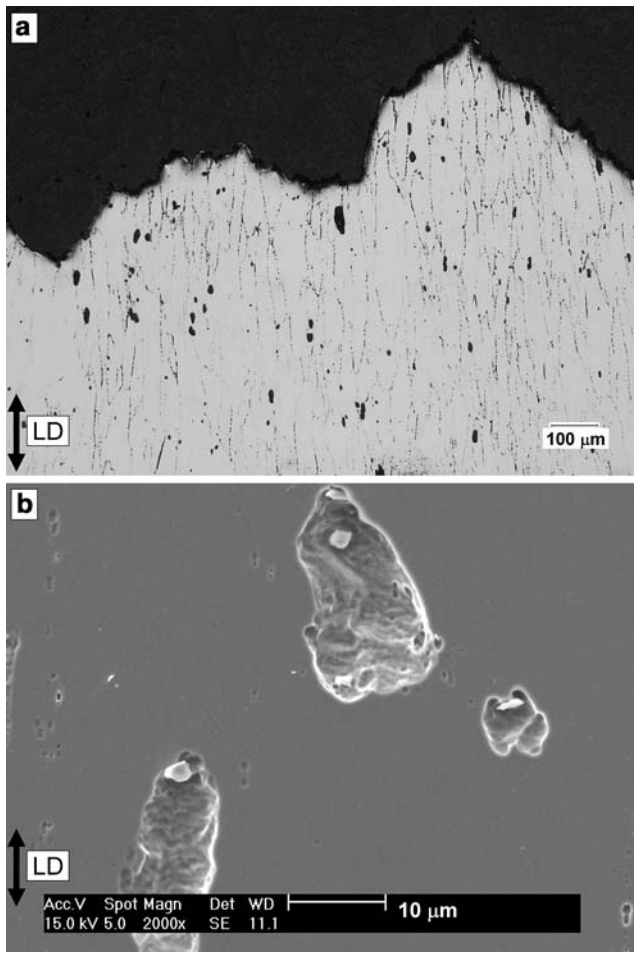

Fig. 10 Cross-sections near the fracture surface of (a) a σ-free tensile sample (light optical microscope image) and (b) a σ-free sample exhibiting microvoids (scanning electron microscope image). Note that the loading direction (LD) is indicated

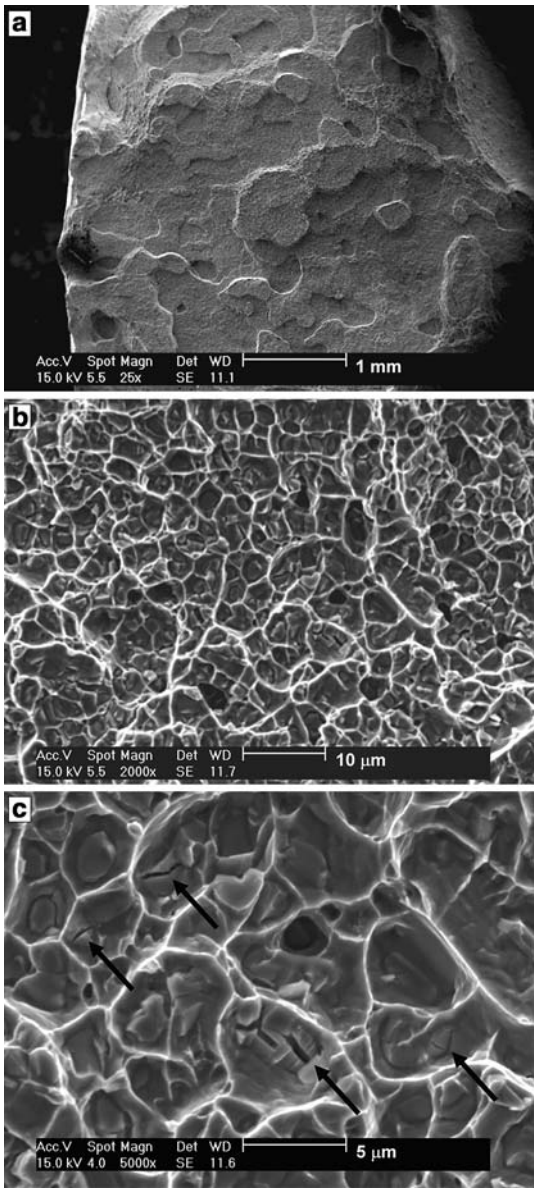

Fig. 11 Scanning electron microscope images of the fracture surface appearance for (a) a σ-containing tensile sample exhibiting several plateaus, (b) a σ-free tensile sample exhibiting ductile fracture appearance, and (c) a σ-containing tensile sample fracture surface showing cracked sigma particles within each void

attributed to premature cracking of the σ-phase particles and preferential crack growth on planes of high particle content associated with microstructural "bands." The current work adds to this by showing that the reduced ductility is largely due to the presence of packets containing σ-phase and not solely due to the short-transverse orientation, since the tensile properties were shown to decrease when the σ-phase packets were present in the samples over the σ-free condition.

The role of the particles on the fracture process in the short-transverse sample orientation can be summarized as follows. The σ-phase particles crack while the matrix is still plastically deforming, presumably at larger particles first, followed by smaller ones. If σ-phase packets are not present, as in the σ-free samples, the matrix austenite grains can undergo extensive plastic deformation, creating micro-voids around whatever

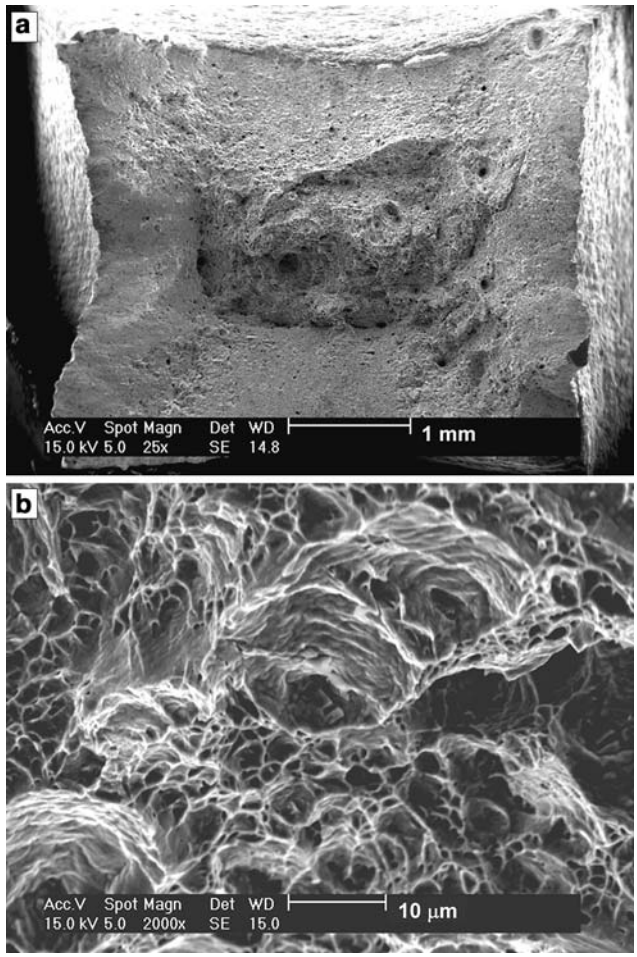

Fig. 12 Scanning electron microscope images showing (a) the ductile fracture surface appearance of the σ-free tensile sample and (b) the appearance of microvoid coalescence on the σ-free tensile sample fracture surface showing a few particles within respective voids

particles are present and leading to a typical microvoid coalescence fracture mechanism. In this case, the particles do not play a large role in the fracture process, and the strength and ductility values are consistent and relatively high. If σ-phase packets are present, the adjacent σ-phase particles that are cracked leave little surrounding matrix material between them to support further stress, leading to rapid microvoid coalescence along the plane of a σ-phase packet. Since the σ-phase packets do not occur on the same plane, the crack formed during fracture will change planes if the end of a packet is encountered to allow the crack to propagate in the same direction, but along a plane of easier crack extension.

4. Conclusions

The presence of microstructural "packets" of σ-phase particles in AL-6XN plate material has a deleterious effect on the fracture toughness and tensile properties in the through-thickness (short-transverse) direction. The reduction in toughness and tensile properties can be attributed to particle cracking within the σ-phase packets that leads to premature fracture. This limits the ability of the material to plastically deform and

work harden, which accounts for the observed reductions in ductility, toughness, and ultimate tensile strength.

Acknowledgments

This work was supported by the Office of Naval Research, under Contract No. N00014-00-1-0448. The authors would also like to thank Dr. Tom Lienert at Los Alamos National Laboratory in Los Alamos, NM, USA for conducting the electron beam welding procedures, Keith Donald at Fracture Technology Associates in Bethlehem, PA, USA for conducting the fracture toughness tests, Arlan Benscoter for assistance in metallography, and Mike Rex for assistance in sample preparation.

References

1. A.J. Sedriks, *Corrosion of Stainless Steels*, Wiley, 1996
2. A.C. Stauffer, D.A. Koss, and J.B. McKirgan, Microstructural banding and failure of a stainless steel, *Metall. Mater. Trans. A*, 2004, **35A**(4), p 1317–1324
3. S.W. Banovic, J.N. DuPont, and A.R. Marder, Dilution and microsegregation in dissimilar metal welds between super austenitic stainless steel and nickel base alloys, *Sci. Technol. Welding Joining*, 2002, **7**(6), p 374–383
4. Q.G. Wang, Microstructural effects on the tensile and fracture behavior of aluminum casting alloys A356/357, *Metall. Mater. Trans. A*, 2003, **34A**(12), p 2887–2899
5. W.H. Hunt, J.R. Brockenbrough, and P.E. Magnusen, An Al–Si–Mg Composite Model System: Microstructural Effects on Deformation and Damage Evolution, *Scr. Metall. Mater.*, 1991, **25**(1), p 15–20
6. Standard test method for linear-elastic plane-strain fracture toughness K_{IC} of metallic materials, E 399, *Annual Book of ASTM Standards*, American Society for Testing and Materials
7. Standard test methods for tension testing of metallic materials, E 8-04, *Annual Book of ASTM Standards*, American Society for Testing and Materials
8. Test method for measurement of fracture toughness, E 1820–05, *Annual Book of ASTM Standards*, American Society for Testing and Materials
9. J.A. Joyce and J.P. Gudas, in *Manual on Elastic-Plastic Fracture: Laboratory Test Procedures*, American Society for Testing and Materials, 1996
10. D. Broek, *Elementary Engineering Fracture Mechanics*, Sijthoff & Noordhoff, 1978
11. M.J. Perricone and J.N. DuPont, Effect of composition on the solidification behavior of several Ni–Cr–Mo and Fe–Ni–Cr–Mo alloys, *Metall. Mater. Trans. A*, 2006, **37A**(4), p 1267–1280